https://doi.org/10.1016/j.chemphyslip.2019.104827

Enhanced chain packing achieved via putative headgroup ion-triplet formation in binary anionic lipid / cationic surfactant mixed monolayers

Christian Wölk[1], Gerd Hause[2], Olof Gutowski[3], Richard D. Harvey[1,*], Gerald Brezesinski[4]

[1]*Institute of Pharmacy, Martin-Luther-Universität Halle-Wittenberg, Halle (Saale), Germany*
[2]*Biozentrum, Martin-Luther-University Halle-Wittenberg, Halle (Saale), Germany*
[3]*Deutsches Elektronen-Synchrotron (DESY), 22607 Hamburg, Germany*
[4]*Max Planck Institute of Colloids and Interfaces, Am Mühlenberg 1, 14476 Potsdam, Germany*

*Corresponding author. E-mail: richard.harvey@pharmazie.uni-halle.de

https://doi.org/10.1016/j.chemphyslip.2019.104827

Abstract

Lipid/surfactant miscibility was investigated in monolayers composed of binary mixtures of dipalmitoylphosphatidylglycerol (DPPG) and dihexadecyl dimethylammonium bromide (DHDAB). Langmuir monolayers formed from biomimetic DPPG/DHDAB mixtures based on the anionic:cationic lipid ratios observed in the bacterium *Staphylococcus aureus* (7:3 and 1:1) were examined alongside those of the pure amphiphiles and a surfactant rich 3:7 mixture. Using a combination of GIXD, TRXF and IRRAS, DPPG/DHDAB 1:1 monolayers were found to form a more stabilised condensed phase compared to pure DPPG, which was composed entirely of electrostatically neutral ion pairs, analogous to the so-called catanionic amphiphiles spontaneously formed by single-chain surfactants with opposing headgroup charges. Despite the lack of lateral charge repulsion the ion paired phase of DPPG/DHDAB exhibited slightly looser chain packing that was observed for DPPG indicating a significant steric effect on packing geometry caused by ion pair formation. Surprisingly, the 7:3 mixture of DPPG/DHDAB formed an completely condensed phase, with no isotherm transitions, in which the chain packing was significantly closer than was found for either DPPG or the totally ion paired monolayer. It is postulated that this mixture forms a distinct DPPG/DHDAB/DPPG ion triplet phase in which the overall negative charge is delocalised across the headgroups. Vesicles composed from the 7:3 mixture formed highly stable dispersions with an increased gel to liquid crystalline phase transition temperature with respect to its pure components. Increasing the proportion of DHDAB above 50 mol% led to demixing between the condensed ion paired phase and the more fluid surfactant, as was clearly observed in epifluorescence images taken of the surface films.

https://doi.org/10.1016/j.chemphyslip.2019.104827

Keywords

Catanionic monolayers; DHDAB; DPPG; ion pair; ion triplet; Staphylococci

https://doi.org/10.1016/j.chemphyslip.2019.104827

Graphical Abstract

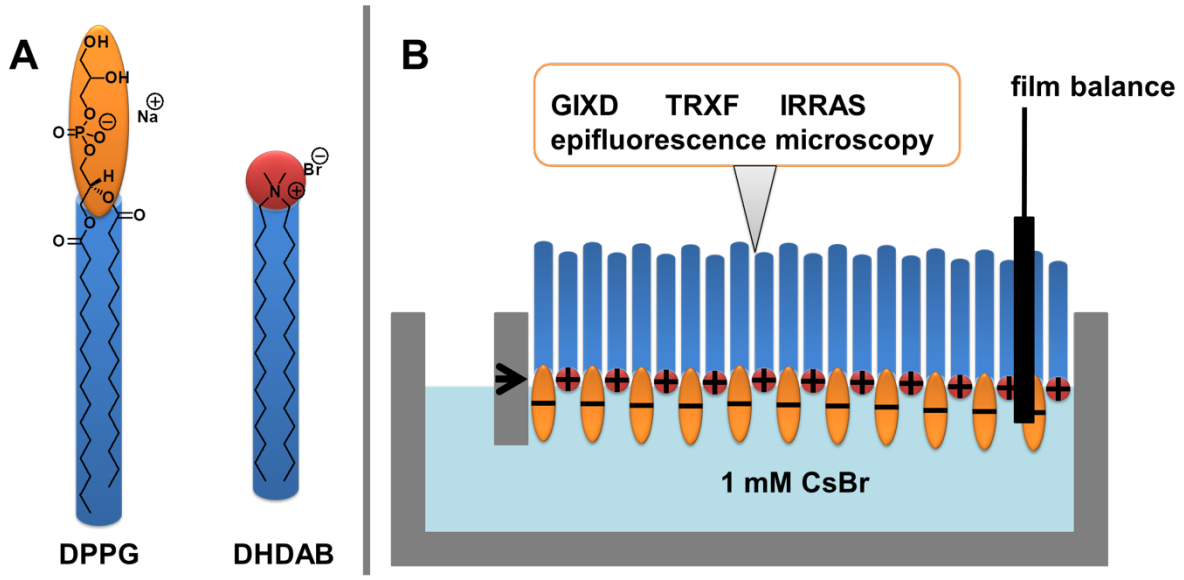

https://doi.org/10.1016/j.chemphyslip.2019.104827

1 Introduction

The study of lipids or surfactants in mixed amphiphile systems, is often used to model the complex compositions of biological membranes and their interactions with intrinsic and extrinsic materials such as proteins, peptides and drug molecules (Peetla et al., 2009; Sebaaly et al., 2019). One application of such biomimetic studies has been in the investigation of mixtures of differently charged amphiphiles, to produce biocompatible colloidal encapsulation and delivery systems with tunable surface properties, facilitating improved dispersion stability, optimized drug or nucleic acid loading, triggered payload release and targeting (Dhawan and Nagarsenker, 2017; Gonçalves Lopes et al., 2019). Vesicles formed from binary mixtures of monoalkyl cationic and anionic surfactants, which form distinct ion-pair complexes, are considered particularly attractive as cheaper alternatives to phospholipids for drug delivery (Dhawan and Nagarsenker, 2017). Of course a major problem with producing neutral vesicles from equimolar mixtures of oppositely-charged surfactants, is that their dispersions need to be stabilized by additional components such as cholesterol or by the adsorption of polymers (Kuo and Chang, 2016, 2015). These additional formulation ingredients may give rise to unnecessary complexities, and although an obvious solution may be to ensure that one of the charged components is present in excess (Gonçalves Lopes et al., 2019; Kuo and Chang, 2016), the success of such a strategy is dependent upon the miscibility of the components at different ratios.

Looking to nature may also provide useful insights into the properties of cat/anionic lipid mixtures, specifically the phospholipid components of the *Staphylococcus aureus* plasma membrane. This is a rich source of the aminoacyl lipid lysyl-phosphatidylglycerol (L-PG), which is cationic in the mildly acidic environment of the *S. aureus* membrane outer leaflet (Collins and Hamilton, 1976; Tocanne et al., 1974). When cultured at neutral pH, in the absence of environmental stressors, the phospholipid compositions of different *S. aureus* strains (lacking specific envelope mutations) comprise between 20 and 40% L-PG mixed predominantly with anionic phosphatidylglycerol (PG) (55 – 75%) and cardiolipin (CL) (~5%) (Ernst et al., 2018; Gould and Lennarz, 1970; Rehal et al., 2017). Environmental stresses such as mild acidity or the presence of antimicrobial peptides leads to an increase in L-PG

biosynthesis (Andra et al., 2011; Gould and Lennarz, 1970; Peschel et al., 2001) which alters membrane charge and rigidity to resist the stress (Rehal et al., 2017; Roy, 2009). Due to its high alkali lability (Danner et al., 2008), using native L-PG to study the behavior of mixed systems with PG is problematic, and has been more successfully achieved using chemically stable L-PG analogues (Cox et al., 2014; Rehal et al., 2019). Simple systems using cationic surfactants in lieu of L-PG are also useful because they allow the study of lipid miscibility and structure in *S. aureus* membrane models at neutral pH (Hubbard et al., 2017; Schmid et al., 2018).

Using various binary mixtures of dipalmitoyl-PG and the cationic surfactant dihexadecyldimethylammonium bromide (DHDAB), as a crude *S. aureus* inspired model, we have previously shown that a biomimetic mixture containing 30 mol% DHDAB exhibited a greater melting transition temperature than an equimolar mixture (Schmid et al., 2018). This led us to speculate on the molecular interactions between the anionic lipid and cationic surfactant, firstly whether neutralization of DPPG/DHDAB 1:1 vesicles resulted from true ion pairing, and secondly whether putative ion triplet formation in DPPG/DHDAB 2:1 mixtures, was responsible for their increased thermal stability. Air/liquid interface Langmuir monolayers have previously been used to study the thermodynamics of mixing of anionic phospholipids and cationic surfactants (Panda et al., 2010; Roy et al., 2014; Sung et al., 2010), and therefore constitute a useful system for comparing DPPG/DHDAB mixtures of interest, whilst circumventing the need for an excess of one charge to ensure vesicle stability. These mixed monolayers can be used as a platform for a variety of techniques designed to examine their structural and interfacial physicochemical properties. In this study, DPPG/DHDAB monolayer structure and component miscibility have been examined by a combination of grazing-incidence x-ray diffraction (GIXD), infrared reflection-absorption spectroscopy (IRRAS) and epifluorescence microscopy. Additionally, total reflection x-ray fluorescence (TRXF) was used to determine the composition of the electric double layer at the monolayer interface, in order to elucidate the surface charge in a more precise way than could be achieved by measuring the zeta potential of dispersed vesicles. Our findings indicate distinct differences between the 1:1 and 2:1 DPPG/DHDAB mixtures, which provide further evidence for an increased stabilization achieved via ion triplet formation. Not only do these results have interesting implications for studying the

https://doi.org/10.1016/j.chemphyslip.2019.104827

effects of environmental stress on *S. aureus* membranes, but they may also help in the design of highly stable surfactant-based drug and nucleic acid delivery systems.

https://doi.org/10.1016/j.chemphyslip.2019.104827

2 Material and Methods

2.1 Materials

Dipalmitoyl-*sn*-glycero-3-phospho-(*rac*-1-glycerol) sodium salt (DPPG) was supplied by Avanti Polar Lipids (Alabaster, AL, USA) and dihexadecyldimethylammonium bromide with a purity of 97% was purchased from Sigma Aldrich. The fluorescent dye BODIPY 558/568 C12 (4,4-difluoro-5-(2-thienyl)-4-bora-3a,4a-diaza-*s*-indacene-3-dodecanoic acid) (λ_{ex}^{max} = 558 nm, λ_{em}^{max} = 568 nm) was purchased from ThermoFisher Scientific. CsBr (purity 99.999 %), chloroform and methanol were purchased from Sigma Aldrich. For aqueous solutions Milli-Q Millipore water with a specific resistance of 18.2 MΩ·cm was used.

2.2 Methods

2.2.1 Langmuir Isotherms

The lipid monolayers were examined on a custom-made computer-interfaced Langmuir film balance (Riegler & Kirstein, Potsdam, Germany) at a compression rate of ≤10 Å²·(molecule·min)$^{-1}$. Using the Wilhelmy method, the surface pressure was measured with a roughened glass plate with an accuracy of ±0.1 mN·m^{-1}, and the area per molecule with an accuracy of ±0.5 Å². A connected thermostat was kept at 20 °C with a precision of ± 0.1 °C. Lipid solutions in chloroform, at a concentration of 1 mM, were spread carefully from a micro-syringe (Hamilton, Switzerland) onto the aqueous subphases. Before compression, 10 min were given for the evaporation of the organic solvent. All isotherms were measured at least twice for reproducibility.

2.2.2 Infrared reflection-absorption spectroscopy (IRRAS)

IRRAS is based on the specific absorption of electromagnetic waves leading to the vibration of atoms or groups of atoms. The decrease of the reflected intensity at the specific energy can be quantified. The single-beam infrared reflectance spectra were recorded by means of a Vertex 70 FT-IR spectrometer (Bruker, Germany) equipped with a liquid nitrogen cooled MCT detector. The spectrometer was coupled with a Langmuir film balance (Riegler & Kirstein, Potsdam, Germany) containing two troughs: one for the sample (monolayer) and one for a reference (bare air/water interface). The instrument setup was placed in a sealed container (with an external

air/water reflection unit XA-511, Bruker, Germany) to guarantee a constant vapor atmosphere. The trough temperature was maintained at (20 ± 1) °C by means of a circulation bath. The sample and reference spectra were recorded at an incidence angle of 40° using parallel (p) or vertically (s) polarized IR light (KRS-5 wire grid polarizer). The spectra were recorded with 4 cm^{-1} resolution and co-added over 200 scans for s-polarized light and over 400 scans for p-polarized light. A computer controlled 'trough shuttle system' was used to switch between recording the sample and the reference spectra. In order to eliminate the water signal, the reflection-absorption spectra were calculated as $-\log(R/R_0)$, where R_0 and R are the reflectivities of the bare (reference) and the monolayer-covered (sample) surfaces, respectively. Details about IRRAS can be found in a number of publications (Dluhy et al., 1983; Flach et al., 1997; Mendelsohn et al., 2010, 1995; Mendelsohn and Flach, 2002; Muenter et al., 2008).

2.2.3 Epifluorescence Microscopy

Fluorescence microscopy imaging of monolayers at the air/water interface was performed using an Axio Scope A1 Vario epifluorescence microscope (Carl Zeiss MicroImaging, Jena, Germany) installed above a Langmuir Teflon trough with a maximal area of 264 cm^2 and two moveable computer-controlled Teflon barriers (Riegler & Kirstein, Potsdam, Germany). The trough was positioned on an *x*–*y* stage (Märzhäuser, Wetzlar, Germany) to be able to move the film surface with respect to the objective lens to any desired position. The *x*–*y*–*z* motion control was managed by a MAC5000 system (Ludl Electronic Products, Hawthorne, NY, USA). The trough was enclosed by a home-built Plexiglas hood to ensure a dust-free environment and to minimize evaporation of water. The temperature of (20.0 ± 0.1) °C was maintained with a circulating water bath, and the whole setup was placed on a vibration-damped optical table (Newport, Darmstadt, Germany). The air/water interface was illuminated using the following setup from Carl Zeiss MicroImaging (Jena, Germany): a 100 W mercury arc lamp (HXP 120 C), a long working distance objective (LD EC Epiplan-NEOFLUAR 50×), and a filter/beam splitter combination (Filter Set 81HE), to select appropriate wavelengths for the excitation and detection of BODIPY 558/568 C12. Images were recorded using an EMCCD camera (ImageEM C9100-13, Hamamatsu, Herrsching, Germany). Image analysis and data acquisition were done using the AxioVision software (Carl Zeiss MicroImaging, Jena, Germany). All presented images

show areas of individually contrast-adjusted raw data. Lipid solutions with a concentration of 1 mM lipid in chloroform containing only 0.1 mol % fluorescently labeled BODIPY 558/568 C12 were prepared separately. The monolayer was compressed using a compression speed of 2 $Å^2 \cdot molecule^{-1} \cdot min^{-1}$. Microscopy images were taken during the compression of the monolayer.

2.2.4 Grazing incidence X-ray diffraction (GIXD)

The GIXD experiments were performed at the high resolution diffraction beamline P08 (PETRA III, DESY, Hamburg, Germany). The temperature controlled Langmuir trough (Riegler & Kirstein, Potsdam, Germany) was located in a hermetically sealed container with Kapton windows. The trough was constantly flushed with helium (He) to avoid scattering of molecules from the air and to increase the signal to background ratio considerably. The synchrotron beam was monochromated by a set of two monochromators (Silicon double crystal (Si111) and a Germanium double crystal (Ge311)). The photon energy was adjusted to 15 keV corresponding to a wavelength of 0.827 Å. The footprint of the incoming beam on the monolayer surface is approximately 2 mm × 50 mm. The incident angle was adjusted to 0.07° to be below the critical angle for total external reflection for water. A glass block in the subphase just beneath the illuminated area of the monolayer reduced mechanically excited surface waves. The diffraction signal was measured with a vertically-oriented position-sensitive (PSD) detector (MYTHEN, microstrip system for time resolved experiments, DECTRIS, Baden, Switzerland) rotating around. A Soller collimator (JJ X-RAY, Denmark) was located between the sample and the detector to restrict the in-plane divergence of the diffracted beam to 0.09°. Details of GIXD are described in literature (Als-Nielsen et al., 1994; Jacquemain et al., 1992; Kaganer et al., 1999; Kjaer, 1994; Stefaniu and Brezesinski, 2014).

The representation of the diffraction peaks performed using a MatLab macro. Model peaks taken as Lorentzian in the in-plane (Bragg peaks, Q_{xy}) and Gaussian in the out-of-plane direction (Bragg rods, Q_z) were fitted to the integrated data. The obtained Bragg peak positions and centers of the Bragg rods give structure relevant information.

The in-plane coherence length L_{xy} can be approximated from the experimentally determined full-width at half-maximum (FWHM) of the Bragg peak using L_{xy}~0.9(2π)/fwhm(Q_{xy}) with the resolution corrected fwhm(Q_{xy})=√[(FWHM)^2+(0.012)^2].

2.2.5 Total reflection x-ray fluorescence (TRXF)

During the last years, TRXF has been established as an element-specific complementary scattering technique (Bu and Vaknin, 2009; Daillant et al., 1991; Shapovalov et al., 2007). TRXF measurements were carried out at the beamline P08 (PETRA III, DESY, Hamburg, Germany) using the above described setup. The fluorescence signal was detected by an Amptek X-123 SDD detector (Amptek, Bedford, United States of America) placed almost parallel to the liquid surface and perpendicular to the photon beam axis. The footprint center of the incident beam was adjusted to the middle of the trough at the centre of the view angle of the fluorescence detector. The TRXF-ray spectra were analyzed by fitting multiple Gaussian functions to the specific fluorescence lines of each element. The experimentally determined fluorescence intensity from the adsorbed ions can be interpreted quantitatively either by a calibration procedure utilizing monolayers with known charge density or by calibration with respect to the bare aqueous surface (Brezesinski and Schneck, 2019).

2.2.6 CryoTEM

Lipid dispersions were prepared using the thin film rehydration procedure. Accordingly, the lipids were dissolved in chloroform/methanol (9:1, v/v) and combined at the molar ratio DPPG/DHDAB 7:3. Lipid films were obtained by evaporating the solvent for 1 h at 200 mbar and for a further 3 h at 10 mbar. After evaporation, water was added to give a stock dispersion (2 mg mL^{-1}). The lipid formulations were incubated at 50 °C while shaking (1400 rpm, 30 min), followed by bath sonication (37 kHz, 50 °C, 3 min). Afterwards the lipid dispersion was treated by extrusion through a 200 nm polycarbonate membrane (Avestin Europe GmbH, Mannheim, Germany) at 60°C using a LiposoFast^{TM} extruder (Avestin Europe GmbH, Mannheim, Germany).

Vitrified specimens were prepared using a blotting procedure, performed in a chamber with controlled temperature and humidity using an EM GP grid plunger (Leica, Wetzlar, Germany). The sample dispersion (6 µL) was placed onto an EM

https://doi.org/10.1016/j.chemphyslip.2019.104827

grid coated with a holey carbon film (C^{flat}, Protochips Inc., Raleigh, NC). Excess solution was then removed by blotting with a filter paper to leave a thin film of the dispersion spanning the holes of the carbon film on the EM grid. Vitrification of the thin film was achieved by rapid plunging of the grid into liquid ethane held just above its freezing point. The vitrified specimen was kept below 108 K during storage, transferred to the microscope and investigated. Specimens were examined with a Libra 120 Plus transmission electron microscope (Carl Zeiss Microscopy GmbH, Oberkochen, Germany), operating at 120 kV. The microscope was equipped with a Gatan 626 cryotransfer system. Images were acquired using a BM-2k-120 dual-speed on-axis SSCCD camera (TRS).

https://doi.org/10.1016/j.chemphyslip.2019.104827

3 Results

Surface-sensitive synchrotron X-ray scattering and spectroscopic experiments were performed to explore the characteristics of Langmuir monolayers of oppositely charged mixed amphiphiles. The premixed solutions were spread as monolayers at the gas/liquid interface on water containing monovalent salt solutions, revealing that the negatively charged DPPG and the positively charged DHDAB head groups are miscible over a large range of compositions and form a nearly neutral surface in the 1:1 mixture.

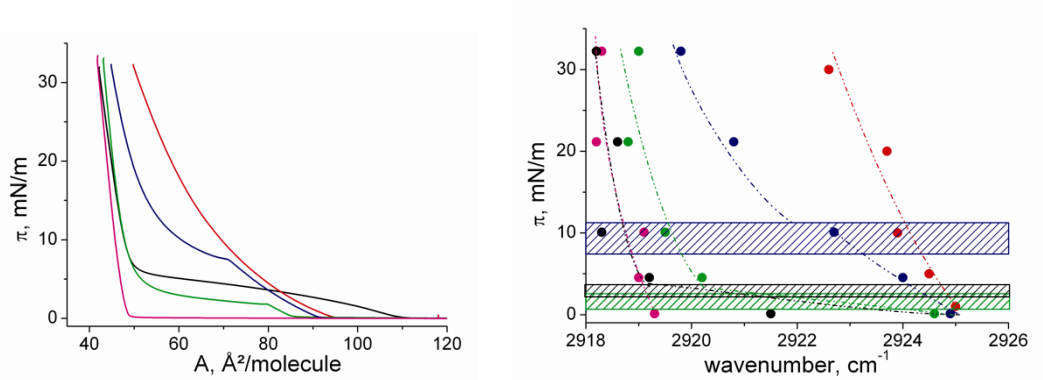

Fig. 1. Left: Pressure-area isotherms of DPPG (black), DHDAB (red) and the DPPG/DHDAB mixtures 7:3 (magenta), 1:1 (green) and 3:7 (blue). Right: The corresponding wavenumbers of the asymmetric CH_2 stretching vibration taken at different lateral pressures along the isotherms. The corresponding plateau region, observed in the isotherms of DPPG, DPPG/DHDAB 7:3 and DPPG/DHDAB 1:1, is indicated.

The isotherm of DHDAB (red) has a shape characteristic for monolayers in the liquid-expanded (LE) state (Fig. 1). The molecular area decreases continuously with increasing pressure without any indication of a phase transition (plateau region or kink). This is supported by the values of the asymmetric CH_2 stretching vibration (ν_{asym}) obtained in IRRAS experiments along the isotherm (Fig. 1, spectra presented in Supporting Information Fig. S1). The values between 2926 and 2924 cm^{-1} indicate a high amount of *gauche* conformers. Only at the highest pressure of 30 mN/m, the value is with 2923 cm^{-1} already typical for lipids in the transition range between LE and liquid-condensed (LC). DPPG (black) exhibits a first-order phase transition, which starts around 3 mN/m (Fig. 1). The transition is characterized by a pronounced plateau region in which the LE and LC phases coexist. At lower pressures, the lipid

layer is in the LE phase with higher v_{asym} numbers. The epifluorescence micrograph shows a homogeneous background with no domains (data not shown). In the plateau area, circular and kidney shaped LC domains can be seen in coexistence with the LE phase (Fig. 2). Above the plateau region, wavenumbers of the $v_{asym}(CH_2)$ band between 2919 and 2918 cm^{-1} indicate a tightly packed LC phase. Adding DHDAB to DPPG leads to pronounced changes which are based on electrostatic and van der Waals forces. The isotherm of the DPPG/DHDAB 7:3 mixture (magenta) is completely condensed with no phase transition (Fig.1). The corresponding wavenumbers between 2919 and 2918 cm^{-1} are typical for a tightly packed condensed state. Even if the differently charged head groups are not balanced (a net negative charge is expected), the addition of a molecule which does not form a condensed monolayer by itself improves the lateral packing in the mixed layer. The 1:1 mixture (Fig.1, green) with perfectly balanced charged head groups exhibits again a plateau region which is below the one of pure DPPG indicating a slight stabilization of the condensed state. In the plateau region circular domains were observed (Fig. 2) indicating dominating line tension at the LC/LE border which can be expected in an electrically neutral ion pair mixture with balanced electrostatic repulsion between the molecules in the LC phase. As can be seen in Fig. 1 (right), the $v_{asym}(CH_2)$ values in the LC phase are with 2920-2919 cm^{-1} slightly higher than the ones of DPPG and the 7:3 mixture indicating a less tight packing in the electrostatically balanced 1:1 mixture. The DPPG/DHDAB 3:7 mixture exhibits a plateau region in the isotherm around 9 mN/m (Fig. 1). In the plateau region, the LC domains have a flower shape (Fig. 2). This may result from the now dominating electrostatic interactions overcoming the line tension. The predominance of liquid-like DHDAB leads to the stabilization of the LE phase, but the 30 mol% of DPPG allow the formation of a condensed phase. However, the $v_{asym}(CH_2)$ values are with 2921-2920 cm^{-1} clearly higher indicating more rotational freedom of the chains.

https://doi.org/10.1016/j.chemphyslip.2019.104827

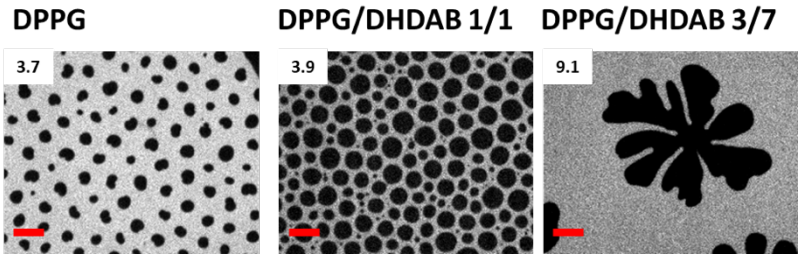

Fig. 2. Fluorescence microscopy images of monolayers of DPPG and DPPG/DHDAB mixtures (n/n) on 1 mM CsBr subphase at selected surface pressures (number in the left upper corner $mN \cdot m^{-1}$) in the LE/LC transition plateau of the isotherms. The red scale bar indicating 20 μm is the same for all pictures. The fluorescent lipid probe was BODIPY 558/568 C12 in a concentration of 0.1 mol %.

The in-plane structure of condensed phases can be determined by GIXD on an Angstrom level.

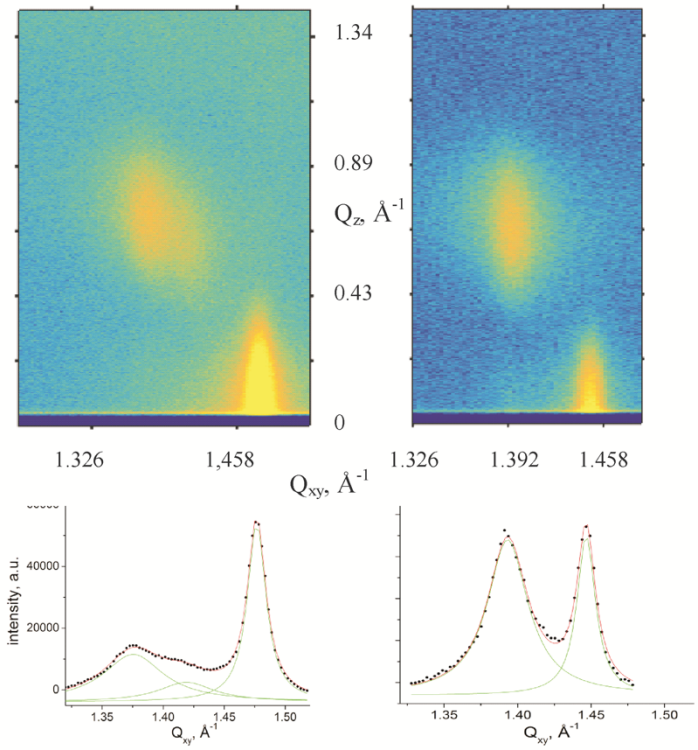

Fig. 3. GIXD data of DPPG (left) and DPPG/DHDAB 1:1 (right) at 10 mN/m. Top: The diffracted intensity is plotted as contour plot of the diffraction intensities as a function of the in-plane Q_{xy} and out-of-plane Q_z components of the scattering vector. Bottom: The diffracted intensity is plotted as a function of the in-plane scattering vector component Q_{xy} (Bragg peak). The points are the experimentally observed data and the lines are the Lorentzian fits to the data.

The monolayer of DPPG is characterized by three diffraction peaks above the horizon ($Q_z > 0$) in the wide-angle region (at high Q_{xy}) at all lateral pressures

investigated. Three Bragg peaks are typical for an oblique lattice structure of tilted chains ($t \sim 30°$, Fig. 3 left). The Bragg peak positions, their full-widths at half-maximum and all lattice parameters obtained for DPPG and the different mixtures at 20 °C and different surface pressures are listed in Supporting Information Tables S1-S5. Lateral compression to higher surface pressure π does not change the lattice type but leads to a decrease of the tilt angle *t*. The small cross-sectional chain area of A_0 = 19.5 Å^2 indicates tight packing with drastically reduced rotational freedom. Plotting 1/cos(*t*) vs. the lateral pressure and extrapolating to zero tilt angle allows the determination of the tilting transition pressure (Supporting Information Figure S2). This procedure is based on the fact that the condensed part of the isotherms exhibits linear relations between pressure and molecular area. The only assumption to be made is a constant cross-sectional area A_0 in the LC phase what is justified looking at the GIXD data (see tables in Supporting Information) (Bringezu et al., 2002). The extrapolated value (50.5 mN·m^{-1}) is quite high and has not been experimentally determined. The maximum tilt angle was determined by the extrapolation to zero surface pressure and is slightly depending on the mole fraction in the mixtures (Supporting Information Fig. S3).

A modified Landau theory predicts that the tilt contribution to the distortion is proportional to sin^2(t) (Kaganer and Loginov, 1995). Plotting the lattice distortion *d* versus sin^2(*t*) and extrapolated to zero tilt allows the separation of the contribution of the tilt from other contributions, such as herringbone packing or chirality, to the lattice distortion (Figure S4) (Kaganer et al., 1999). The determined d_0 value is slightly smaller than 0 (-0.02164). Such small value could be the weak contribution of chirality on the lattice distortion.

DHDAB was measured at 30 mN·m^{-1}. In accordance with the isotherm and IRRAS experiments, only a halo at 1.337 Å^{-1} can be seen in the contour plot typical for fluid chains with a cross-sectional area of 25.5 Å^2 corresponding to an in-plane area of 51 Å^2 per DPPC molecule in perfect agreement with the isotherm data.

Adding 30 mol% of the fluid DHDAB to the condensed DPPG changes the monolayer structure. Two Bragg peaks, characterizing an orthorhombic unit cell, are observed (Fig. 3 right). One Bragg peak is at the horizon and the second one at larger Q_z values typical for a so-called L_2 phase (tilt and distortion to the nearest neighbor). The cross-sectional area is with 19.8 Å^2 only slightly larger compared to that of DPPG. This supports the observation that the $\nu_{asym}(CH_2)$ values are virtually the

same for DPPG and the 7:3 mixture. The condensed phase is clearly stabilized by the 30 mol% of DHDAB. The tilt angle of the chains is smaller, and even the transition pressure into the non-tilted state is slightly decreased (48.3 $mN \cdot m^{-1}$). The extrapolated d_0 value is also smaller (-0.01248). Increasing the percentage of DHDAB in the mixture to 50 mol% does not change the phase type (orthorhombic unit cell) but the packing properties. The cross-sectional area is with 19.8 $Å^2$ similar but the $v_{asym}(CH_2)$ values are slightly larger. The transition pressure into the non-tilted state is distinctly increased (57 $mN \cdot m^{-1}$). The d_0 value (-0.02063) is similar to that of DPPG. Further addition of DHDAB (70 mol%) leads to the re-appearance of the oblique lattice structure but with a much larger cross-sectional area of 20.1 $Å^2$ typical for a rotator phase in perfect agreement with the 2921-2920 cm^{-1}.

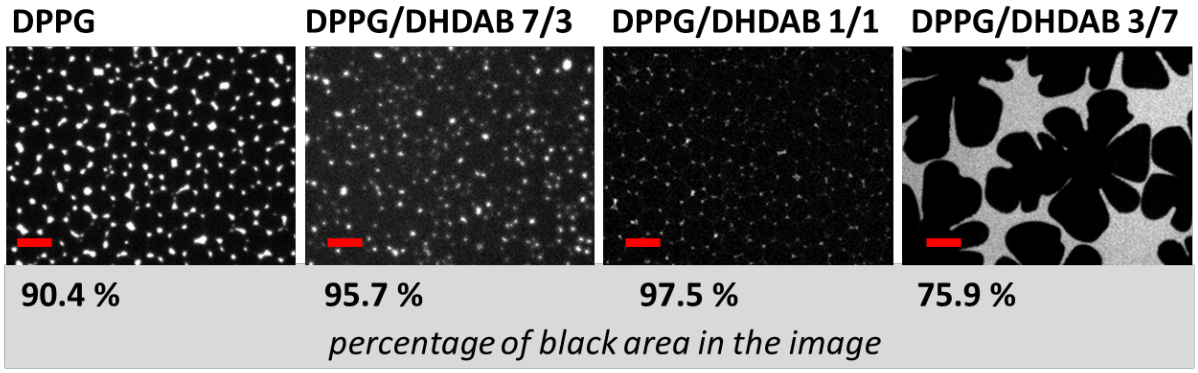

Fig. 4. Fluorescence microscopy images of DPPG and DPPG/DHDAB mixture (n/n) monolayers on 1 mM CsBr subphase at 30 $mN \cdot m^{-1}$) in the LE/LC transition plateau of the isotherms. The red scale bar indicating 20 µm is the same for all pictures. The numbers below the images are the quantified black areas (LC phase) in % determined with the Fiji software (Schindelin et al., 2012). The fluorescent lipid probe was BODIPY 558/568 C12 in a concentration of 0.1 mol %.

The higher wavenumbers observed for the asymmetric CH_2 stretching vibration for the DPPG/DHDAB 3:7 mixture could be based on a partial demixing of the system into a fluid DHDAB rich phase and a condensed DPPG/DHDAB mixture. The observed band position is reflecting an average value between liquid-like and solid-like chains. If the epifluorescence images of all monolayers in the LC phase were evaluated at 30 $mN \cdot m^{-1}$ (a pressure well above the corresponding phase transitions, compare Fig. 1), it is obvious that for the DPPG/DHDAB 3:7 the area of the LC phase is with 75.9 % much smaller compared to the other systems with values above 90% LC (Fig. 4). This observation supports the assumed demixing effect into a DHDAB rich LE phase and a LC phase of a condensed DPPG/DHDAB mixture.

https://doi.org/10.1016/j.chemphyslip.2019.104827

The values obtained from isotherm and GIXD experiments were used to construct a phase diagram of the DPPG/DHDAB mixture (Fig. 5).

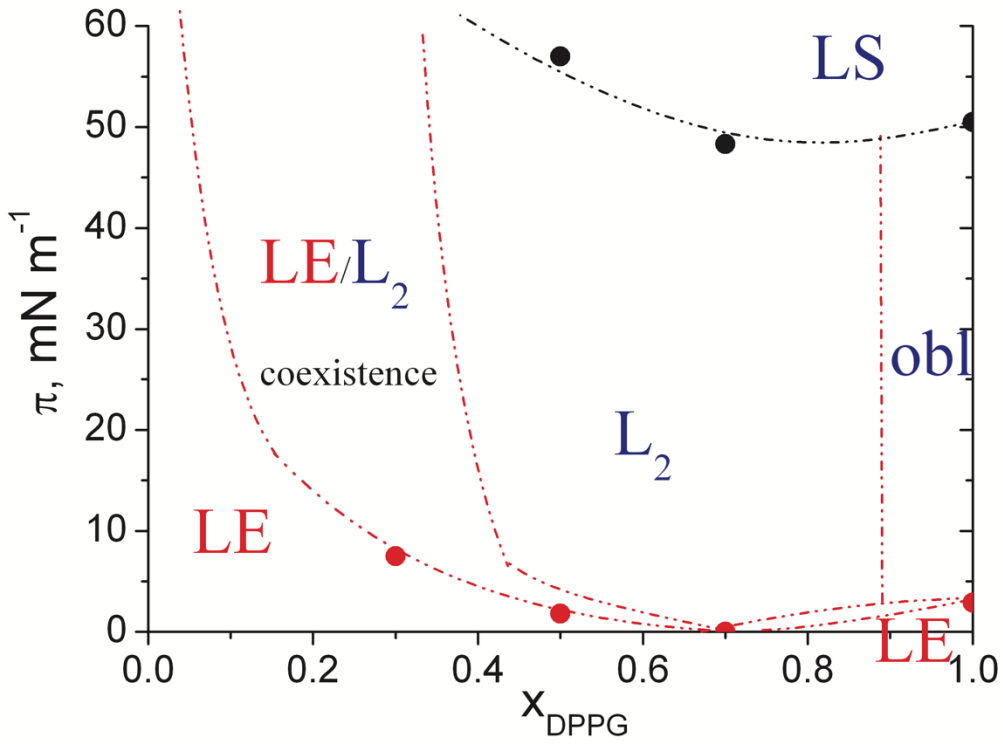

Fig. 5. Phase diagram (lateral pressure π versus the mole-fraction of DPPG) of the DPPG/DHDAB mixture. The phases observed by GIXD are obl (oblique), L_2 (orthorhombic with NN tilt), and LS (non-tilted hexagonal phase). The first-order transition pressures (●) from the disordered LE to an ordered phase are determined by pressure-area isotherms, and the transition pressure into the non-tilted state (●) by extrapolation of the tilt angles determined by GIXD as described in the text.

The charge state of the monolayer was determined by a simple but quantitative TRXF method based on measurements at a single angle of incidence. Since DHDAB has a quaternary ammonium head group, it ensures one permanent positive charge independent from the environmental pH value. In the case of DPPG, the ionization degree depends on the subphase pH. It can be determined by an easy calibration procedure utilizing monolayers with known charge density on subphases containing only one type of counterion to avoid ion competition in the formation of the electrical double layer (EDL). Counterion adsorption to the reference monolayer has to be dominated by unspecific electrostatic attraction and fully charge-neutralizing. A

typical reference for cations is behenylsulfate (BS) containing one charge. However, in the present case we encountered the problem that the used ultrapure water contained traces of calcium (Sturm et al., 2019). These unexpected divalent calcium ions competed with the monovalent cesium for interaction with the negatively charged DPPG. It has been shown in an earlier publication that the phosphate group of DPPG is prone to specific interactions with calcium in contrast to BS (Brezesinski and Schneck, 2019). This is the reason why we cannot quantitatively determine the ionization state of DPPG. However, qualitative conclusions can be clearly drawn.

Fig. 6 presents the most interesting parts of the fluorescence spectra of DPPG, DHDAB, and the corresponding mixtures. The DPPG/DHDAB 3:7 mixed monolayer is effectively positively charged since it attracts bromide counter-ions (~30% compared with the pure DHDAB) and repels the cesium cations (depletion of co-ions in the EDL). This value is slightly lower than the expected one assuming a 1:1 interaction between the negatively charged DPPG and the positively charged DHDAB. For the monolayers containing 50 mol% of DPPG or more, no bromide ions can be seen in the EDL (depletion of co-ions in an effectively negatively charged monolayer). The negatively charged monolayers (DPPG and the 7:3 DPPG/DHDAB mixture) attract the cations from the subphase. Since calcium is a divalent cation, even Ca^{2+} traces can successfully compete with the 1 mM Cs^{+} cations. The amount of cations close to the monolayer decreases with increasing amount of added DHDAB. The 1:1 DPPG/DHDAB mixture does not attract any ions and is therefore a neutral surface.

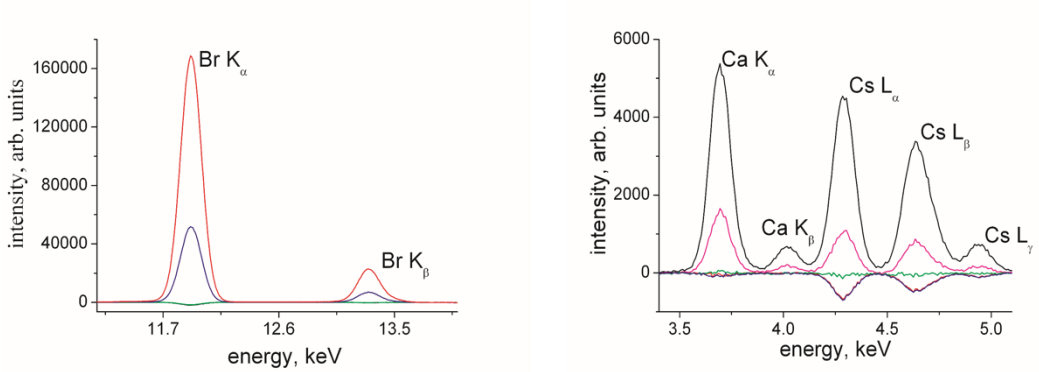

Fig. 6. Selected parts of X-ray fluorescence spectra of DPPG (black), DHDAB (red), and the DPPG/DHDAB mixtures 7:3 (magenta), 1:1 (green) and 3:7 (blue) at a surface pressure of π = 20 mN/m on a subphase containing 1 mM CsBr. The measurements were performed at the P08 synchrotron beamline of PETRA III (DESY, Hamburg, Germany) using a photon energy of 15 keV

(wavelength λ = 0.826 Å) and an angle of incidence of 0.07°. The bands are assigned to the corresponding element.

Interestingly, the complete charge compensation in the 1:1 DPPG/DHDAB mixture does not lead to the highest stabilization of the LC phase and the best packing properties in the monolayer. This is achieved in the 7:3 DPPG/DHDAB mixture with a completely condensed isotherm and the lowest tilting transition pressure. Obviously, not only the charge compensation in ion pairs but additional interactions are important for a dense monolayer packing. We could also confirm in bulk systems, that the DPPG/DHDAB 7:3 mixture has the highest stabilization of the gel phase (liquid crystalline/gel phase transition at ≈ 52 °C) (Schmid et al., 2018). The question arose, if this effect can be turned into a suitable application. One major feature which increases the possible application is the ability to form vesicles. CryoTEM experiments could prove this for the DPPG/DHDAB 7:3 mixture. Vesicles with a diameter equal or smaller to 200 nm can be seen (Fig. 7 A, black arrows). The detailed view shows a shape which is not ideally circular and characterized by edges (Fig. 7 B, white arrows), a morphology which is typical for liposomes in the gel state (Kuntsche et al., 2010).

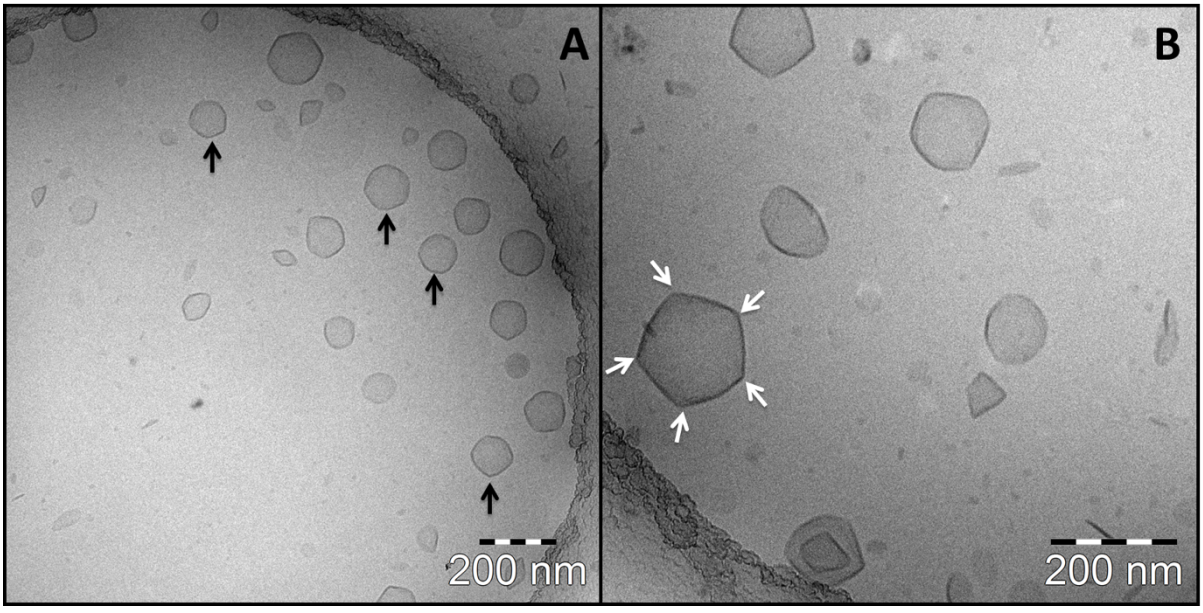

Fig. 7. Cryo-TEM images of DPPG/DHDAB 7:3 2 mg·mL^{-1} in water after extrusion through a 200 nm membrane. The samples were at 22 °C before cryo preparation. Black arrows in (A) indicate exemplary unilamellar vesicles, and white arrows in (B) indicate edges in the vesicular structure.

https://doi.org/10.1016/j.chemphyslip.2019.104827

4 Discussion

With the work presented in this paper and in previously published work (Schmid et al., 2018) DPPG/DHDAB mixtures in different molar ratios have been extensively characterized in both bulk and monolayer systems, with respect to lipid aggregate structure, lipid packing, thermal transitions and charge characteristics. This was necessary to understand the mixing behavior to find the most appropriate mixture to enhance the stability of this system. Both DPPG and DHDAB form lamellar phases in aqueous dispersions, which have a propensity to interdigitate under certain solvent conditions, due to the lateral repulsive effect of their charged headgroups (Tucker et al., 2008; Wilkinson et al., 1987). In the case of DHDAB, its higher aqueous solubility means that vesicle dispersions formed by the surfactant exist in equilibrium with a small concentration of dissolved monomers (Tucker et al., 2008). As is evident from the results of this study, in the form of air/liquid deposited monolayers, the amphiphiles behave quite differently, as DPPG is able to form a condensed layer upon compression, whereas DHDAB exhibits expanded layer characteristics, even at high surface pressure. Furthermore, DHDAB monolayers must be considered as being metastable, due to the solubility of the surfactant leading to a small loss of material into the subphase during compression (Kuo and Chang, 2015). Although both DPPG and DHDAB were in the gel phase at ambient temperature (Adati and Feitosa, 2015; Schmid et al., 2018) the differences in their monolayer compressibility behavior indicates that a mixing gap may be expected somewhere in the binary phase diagram (Sackmann and Demus, 1973), which needed to be taken into account when assessing their miscibility.

Regarding the electrostatic interactions in DPPG/DHDAB mixtures, both our previous zeta potential measurements (bulk system), (Schmid et al., 2018) and the current TRXF measurements (monolayer systems) show that the equimolar mixture gives rise to a neutral interface due to charge compensation, which is indicative of the formation of discrete ion-pairs (Vaknin and Bu, 2010). In mixtures with an excess of either DPPG or DHDAB, appropriate counter ions were again attracted to the interface. However, what is not discernable from studying the charge characteristics of the interface, is whether the ion-pairs were then disrupted, or whether single charged amphiphiles were mixed or phase separated from an ion-paired phase. To

answer this question, we need to examine the evidence from investigations into the packing behavior of the various DPPG/DHDAB mixtures.

The isotherm for the equimolar DPPG/DHDAB mixture showed a reduced surface pressure for the first-order LE/LC phase transition with respect to the pure DPPG monolayer, indicating that there is a stabilization of the condensed phase. The lack of subphase counter ion presence at the interface was indicative of the formation of neutral lipid/surfactant ion-pairs on the surface (Vaknin and Bu, 2010). These DPPG/DHDAB complexes form a distinct condensed phase whose orthorhombic lattice structure was distinct from the oblique packing geometry adopted by pure DPPG in the presence of monovalent counter ions (Maltseva et al., 2006). At 30 $mN \cdot m^{-1}$, the chains of the ion-paired complexes are not as closely packed as those of DPPG monolayers, and despite exhibiting a slightly lower tilt, they require a higher surface pressure than the pure lipid, to achieve a non-tilted hexagonal packing geometry (see Supporting Information figure S2). This suggests that ion-pairing imparts some steric constraints upon the complexes formed, which in the absence of electrostatic lateral repulsion, exerts some restriction upon molecular packing. Nevertheless there is a significant condensing effect of adding an equimolar quantity of DHDAB to DPPG, which has similarly been observed with another similar cationic surfactant dipalmitoyltrimethylammonium propane (DPTAP) (Roy et al., 2014). Indeed the electrostatic attraction between the cationic headgroups of both DAB and TAP surfactants and the phosphate groups of PG and zwitterionic phosphatidylcholine (PC) lipids, exerts similar condensing effects in equimolar mixtures, regardless of any hydrophobic mismatch in the chains, or even the presence of unsaturated surfactants (Chang et al., 2012; Gzyl-Malcher et al., 2011; Panda et al., 2010; Sung et al., 2010; Wu et al., 2014). This is more than likely the result of the spatial proximity of the DAB/TAP quaternary ammonium and the lipid phosphate at the air/water interface, since in the case of PC lipids, the presence of the choline moiety does not appear to compete with the surfactant (Chang et al., 2012; Gzyl-Malcher et al., 2011; Wu et al., 2014).

Although it might be assumed *a priori*, that DPPG/DHDAB ion-pairing in the equimolar mixture would produce the strongest condensing effect, as our results clearly show, this is not the case experimentally. The biomimetic DPPG/DHDAB 7:3

mixture forms a fully condensed phase, with no LE/LC transition, in which the chains are packed in an orthorhombic geometry at 30 $mN \cdot m^{-1}$ with a lower average tilt than the 1:1 mixture or pure DPPG, and according to the IRRAS results, exhibiting the tightest packing. This behavior might be expected to result from the presence of ion pairs, but the entirely miscible excess DPPG apparently leads to the formation of another distinct phase with an improved lateral packing. The reduction in the surface pressure required to achieve non-tilted hexagonal packing (Supporting Information figure S2) also indicates the formation of a highly stable condensed phase, which as we demonstrated facilitates the formation of vesicles with a significantly increased melting transition temperature (Schmid et al., 2018). Enhanced packing efficiency in phospholipid/cationic surfactant mixtures other than those of equal molarity have been observed previously, but were largely uncommented upon. In 2:1 mixtures of both DPPC/DPTAP and DSPC/DHDAB, a greater condensing effect eliciting a smaller area per molecule was achieved, in comparison to 1:1 mixtures (Chang et al., 2012; Gzyl-Malcher et al., 2011). In a mixture more analogous to our own, comprising DPPG and DOTAP, a mixture containing between 20 and 40 mol% cationic surfactant achieved optimal monolayer stability, as demonstrated by a significantly increased collapse pressure (Panda et al., 2010). In a previous publication, we postulated that an ion triplet structure for the DPPG/DHDAB 2:1 mixture (to which the biomimetic 7:3 mixture approximates) (Schmid et al., 2018) might lead to greater bilayer stabilization through more efficient lipid packing. This supposition appears to be fully supported by the data presented here. With the negative charge delocalized between the headgroups in a DPPG/DHDAB/DPPG ion triplet the steric constraints apparent in the ion-pair may be relaxed sufficiently to facilitate the tighter packing observed in the 7:3 monolayer.

In monolayers with approximately twice as much DHDAB as DPPG (the DPPG/DHDAB 3:7 mixture) the isotherm shows that the LE/LC phase transition occurs at a surface pressure far above that of pure DPPG, indicating a stabilization of the LE phase in the presence of excess surfactant. At 30 $mN \cdot m^{-1}$, epifluorescence clearly shows a continued LE/LC phase coexistence, whilst the GIXD data shows characteristics similar to that of the ion paired phase of the DPPG/DHDAB 1:1 mixture. The IRRAS data, averaged from the two phases, also clearly indicates greater rotational freedom of the lipid/surfactant chains. In contrast therefore to the

electrostatically-driven ideal miscibility of the 7:3 and 1:1 mixtures, an excess of DHDAB facilitates phase separation, probably between the ion paired phase and pure surfactant, just as has been observed in different PC/DAB mixtures (Chang et al., 2012; Wu et al., 2014).

What therefore began as an attempt to create a simple synthetic model system for studying lipid-lipid interactions in *S. aureus* membranes (Schmid et al., 2018), has revealed that in catanionic DPPG/DHDAB mixtures, different miscible ratios facilitate the formation of distinct phases. The closer packing of the orthorhombic lattice structure of the 7:3 mixture implies the formation of ion triplets which exhibit less steric hindrance than that observed in the 1:1 ion paired lattice. The applicability of these lipid-surfactant interactions to the natural membrane requires further detailed investigation, however, in a biomimetic mixture of DPPG with an L-PG analogue, membrane order was found to be significantly improved when the ratio of anions to cations was 7:3 (Rehal et al., 2019). With regard to the specific mixing of DPPG with DHDAB in a 7:3 ratio, the formation of colloidally stable dispersions of unilamellar vesicles makes it suitable for use in several drug delivery applications.

Acknowledgement

The authors thank the Deutsches Elektronen-Synchrotron (DESY) for beamtime allocation at P08 and for their excellent technical support.

References

Adati, R.D., Feitosa, E., 2015. The assembly of dialkyldimethylammonium bromide cationic lipids as vesicles or monolayers in presence of poly(ethylene glycol). *Thermochim. Acta* 613, 71–76.

Als-Nielsen, J., Jacquemain, D., Kjaer, K., Leveiller, F., Lahav, M., Leiserowitz, L., 1994. Principles and applications of grazing incidence X-ray and neutron scattering from ordered molecular monolayers at the air-water interface. *Phys. Rep.* 246, 251–313.

Andra, J., Goldmann, T., Ernst, C.M., Peschel, A., Gutsmann, T., 2011. Multiple Peptide Resistance Factor (MprF)-mediated Resistance of *Staphylococcus aureus* against Antimicrobial Peptides Coincides with a Modulated Peptide Interaction with Artificial Membranes Comprising Lysyl-Phosphatidylglycerol. *J. Biol. Chem.* 286, 18692–18700.

Brezesinski, G., Schneck, E., 2019. Investigating ions at amphiphilic monolayers with X-ray fluorescence. Langmuir. https://doi.org/10.1021/acs.langmuir.9b00191

Bringezu, F., Dobner, B., Brezesinski, G., 2002. Generic phase behavior of branched-chain phospholipid monolayers. *Chem. - A Eur. J.* 8, 3203–3210.

Bu, W., Vaknin, D., 2009. X-ray fluorescence spectroscopy from ions at charged vapor/water interfaces. *J. Appl. Phys.* 105. 084911

Chang, C.H., Liang, C.H., Hsieh, Y.Y., Chou, T.H., 2012. Molecular packing and lateral interactions of distearoylphosphatidylcholine with dihexadecyldimethylammonium bromide in Langmuir monolayers and vesicles. *J. Phys. Chem. B* 116, 2455–2463.

Collins, S.H., Hamilton, W.A., 1976. Magnitude of the protonmotive force in respiring *Staphylococcus aureus* and *Escherichia coli. J. Bacteriol.* 126, 1224–1231.

Cox, E., Michalak, A., Pagentine, S., Seaton, P., Pokorny, A., 2014. Lysylated phospholipids stabilize models of bacterial lipid bilayers and protect against antimicrobial peptides. *Biochim. Biophys. Acta -Biomemb.* 1838, 198-2204

Daillant, J., Bosio, L., Benattar, J.J., Blot, C., 1991. Interaction of Cations with a Fatty Acid Monolayer. A Grazing Incidence X-ray Fluorescence and Reflectivity Study. *Langmuir* 7, 611–614.

Danner, S., Pabst, G., Lohner, K., Hickel, A., 2008. Structure and thermotropic behavior of the *Staphylococcus aureus* lipid lysyl-dipalmitoylphosphatidylglycerol. *Biophys. J.* 94, 2150–2159.

Dhawan, V. V., Nagarsenker, M.S., 2017. Catanionic systems in nanotherapeutics – Biophysical aspects and novel trends in drug delivery applications. *J. Control. Release* 266, 331–345.

Dluhy, R.A., Mendelsohn, R., Casal, H.L., Mantsch, H.H., 1983. Interaction of Dipalmitoylphosphatidylcholine and Dimyristoylphosphatidylcholine-d54 Mixtures with Glycophorin. A Fourier Transform Infrared Investigation. *Biochemistry* 22, 1170–1177.

Ernst, C.M., Slavetinsky, C.J., Kuhn, S., Hauser, J.N., Nega, M., Mishra, N.N., Gekeler, C., Bayer, A.S., Peschel, A., 2018. Gain-of-Function Mutations in the Phospholipid Flippase MprF Confer Specific Daptomycin Resistance. *MBio* 9, e01659-18.

Flach, C.R., Gericke, A., Mendelsohn, R., 1997. Quantitative Determination of Molecular Chain Tilt Angles in Monolayer Films at the Air/Water Interface: Infrared Reflection/Absorption Spectroscopy of Behenic Acid Methyl Ester. *J. Phys. Chem. B* 101, 58–65.

Gonçalves Lopes, R.C.F., Silvestre, O.O.F., Faria, A.A.R., C do Vale, M.L., Marques, E.F.E., Nieder, J.J.B., Gonçalves, L.R., Silvestre, O.O.F., Faria, A.A.R., C, do V.M., Marques, E.F.E., Nieder, J.J.B., 2019. Surface charge tunable catanionic vesicles based on serine-derived surfactants as efficient nanocarriers for the delivery of the anticancer drug doxorubicin. *Nanoscale* 11, 5932–5941.

Gould, R.M., Lennarz, W.J., 1970. Metabolism of phosphatidylglycerol and lysyl phosphatidylglycerol in *Staphylococcus aureus. J. Bacteriol.* 104, 1135–1144.

Gzyl-Malcher, B., Filek, M., Brezesinski, G., 2011. Mixed DPPC/DPTAP monolayers at the air/water interface: Influence of indolilo-3-acetic acid and selenate ions on the monolayer morphology. *Langmuir* 27, 10886–10893.

Hubbard, A.T.M., Coates, A.R.M., Harvey, R.D., 2017. Comparing the action of HT61 and chlorhexidine on natural and model Staphylococcus aureus membranes. *J. Antibiot.* 70, 1020–1025.

Jacquemain, D., Wolf, S.G., Leveiller, F., Deutsch, M., Kjaer, K., Als-Nielsen, J., Lahav, M., Leiserowitz, L., 1992. Two-Dimensional Crystallography of Amphiphilic Molecules at the Air–Water Interface. *Angew. Chemie Int. Ed.* 31, 130–152.

Kaganer, V.M., Loginov, E.B., 1995. Symmetry and phase transitions in Langmuir monolayers: The Landau theory. *Phys. Rev. E* 51, 2237–2249.

Kaganer, V.M., Möhwald, H., Dutta, P., 1999. Structure and phase transitions in Langmuir monolayers. *Rev. Mod. Phys.* 71, 779–819.

Kjaer, K., 1994. Some simple ideas on X-ray reflection and grazing-incidence diffraction from thin surfactant films. *Phys. B Phys. Condens. Matter* 198, 100–109.

Kuntsche, J., Freisleben, I., Steiniger, F., Fahr, A., 2010. Temoporfin-loaded liposomes: Physicochemical characterization. *Eur. J. Pharm. Sci.* 40, 305–315.

Kuo, A.-T., Chang, C.-H., 2016. Recent Strategies in the Development of Catanionic Vesicles. *J. Oleo Sci.* 65, 377–384.

Kuo, A.-T., Chang, C.-H., 2015. Elucidating the Effects of Cholesterol on the Molecular Packing of Double-chained Cationic Lipid Langmuir Monolayers by Infrared Reflection-absorption Spectroscopy. *J. Oleo Sci.* 64, 455–465.

Maltseva, E., Shapovalov, V.L., Möhwald, H., Brezesinski, G., 2006. Ionization state and structure of L-1,2-dipalmitoylphosphatidylglycerol monolayers at the liquid/air interface. *J. Phys. Chem. B.* 110, 919-926.

Mendelsohn, R., Brauner, J.W., Gericke, A., 1995. External Infrared Reflection Absorption Spectrometry of Monolayer Films at the Air-Water Interface. *Annu. Rev. Phys. Chem.* 46, 305–334.

Mendelsohn, R., Flach, C.R., 2002. Infrared reflection-absorption spectroscopy of lipids, peptides, and proteins in aqueous monolayers. *Curr. Top. Membr.* 52, 57–88.

Mendelsohn, R., Mao, G., Flach, C.R., 2010. Infrared reflection-absorption spectroscopy: Principles and applications to lipid-protein interaction in Langmuir films. *Biochim. Biophys. Acta - Biomembr.* 1798, 788–800.

Muenter, A.H., Hentschel, J., Borner, H.G., Brezesinski, G., 2008. Characterization of peptide-guided polymer assembly at the air/water interface. *Langmuir* 24, 3306–3316.

Panda, A.K., Vasilev, K., Orgeig, S., Prestidge, C.A., 2010. Thermodynamic and structural studies of mixed monolayers: Mutual mixing of DPPC and DPPG with DoTAP at the air-water interface. *Mater. Sci. Eng.* C 30, 542–548.

Peetla, C., Stine, A., Labhasetwar, V., 2009. Biophysical Interactions with Model Lipid Membranes: Applications in Drug Discovery and Drug Delivery. *Mol. Pharm.* 6, 1264–1276.

Peschel, A., Jack, R.W., Otto, M., Collins, L.V., Staubitz, P., Nicholson, G., Kalbacher,

H., Nieuwenhuizen, W.F., Jung, G., Tarkowski, A., 2001. *Staphylococcus aureus* resistance to human defensins and evasion of neutrophil killing via the novel virulence factor MprF is based on modification of membrane lipids with l-lysine. *J. Exp. Med.* 193, 1067–1076.

Rehal, R., Gaffney, P.R.J., Hubbard, A.T.M., Barker, R.D., Harvey, R.D., 2019. The pH-dependence of lipid-mediated antimicrobial peptide resistance in a model staphylococcal plasma membrane: A two-for-one mechanism of epithelial defence circumvention. *Eur. J. Pharm. Sci.* 128, 43–53.

Rehal, R.P., Marbach, H., Hubbard, A.T.M., Sacranie, A.A., Sebastiani, F., Fragneto, G., Harvey, R.D., 2017. The influence of mild acidity on lysyl-phosphatidylglycerol biosynthesis and lipid membrane physico-chemical properties in methicillin-resistant *Staphylococcus aureus*. *Chem. Phys. Lipids* 206, 60–70.

Roy, H., 2009. Tuning the Properties of the Bacterial Membrane with Aminoacylated Phosphatidylglycerol. *IUBMB Life* 61, 940–953.

Roy, S., Gruenbaum, S.M., Skinner, J.L., 2014. Theoretical vibrational sum-frequency generation spectroscopy of water near lipid and surfactant monolayer interfaces. II. Two-dimensional spectra. *J. Chem. Phys.* 141.

Sackmann, H., Demus, D., 1973. Problems of polymorphism in liquid crystals. *Mol Cryst Liq Cryst* 21, 239–273.

Schindelin, J., Arganda-Carreras, I., Frise, E., Kaynig, V., Longair, M., Pietzsch, T., Preibisch, S., Rueden, C., Saalfeld, S., Schmid, B., Tinevez, J.-Y., White, D.J., Hartenstein, V., Eliceiri, K., Tomancak, P., Cardona, A., 2012. Fiji: an open-source platform for biological-image analysis. *Nat. Methods* 9, 676–82.

Schmid, M., Wölk, C., Giselbrecht, J., Chan, K.L.A., Harvey, R.D., 2018. A combined FTIR and DSC study on the bilayer-stabilising effect of electrostatic interactions in ion paired lipids. *Colloids Surfaces B Biointerfaces* 169, 298–304.

Sebaaly, C., Greige-Gerges, H., Charcosset, C., 2019. Lipid Membrane Models for Biomembrane Properties' Investigation, in: Current Trends and Future Developments on (Bio-) Membranes.

Shapovalov, V.L., Ryskin, M.E., Konovalov, O. V., Hermelink, A., Brezesinski, G., 2007. Elemental analysis within the electrical double layer using total reflection X-ray fluorescence technique. *J. Phys. Chem.* B 111, 3927–3934.

Stefaniu, C., Brezesinski, G., 2014. X-ray investigation of monolayers formed at the

soft air/water interface. *Curr. Opin. Colloid Interface Sci.* 19, 216–227.

Sturm, M., Gutowski, O., Brezesinski, G., 2019. The Influence of Calcium Traces in Ultrapure Water on the Lateral Organization in Tetramyristoyl Cardiolipin Monolayers. *ChemPhysChem* 20, cphc.201900126.

Sung, W., Seok, S., Kim, D., Tian, C.S., Shen, Y.R., 2010. Sum-frequency spectroscopic study of langmuir monolayers of lipids having oppositely charged headgroups. *Langmuir* 26, 18266–18272.

Tocanne, J.F., Ververgaert, P.H.J.T., Verkleij, A.J., van Deenen, L.L.M., 1974. A monolayer and freeze-etching study of charged phospholipids I. Effects of ions and pH on the ionic properties of phosphatidylglycerol and lysylphosphatidylglycerol. *Chem. Phys. Lipids* 12, 201–219.

Tucker, I., Penfold, J., Thomas, R.K., Grillo, I., Barkery, J.G., Mildner, D.F.R., 2008. The surface and solution properties of dihexadecyl dimethylammonium bromide. *Langmuir* 24, 6509–6520.

Vaknin, D., Bu, W., 2010. Neutrally Charged Gas/Liquid Interface by a Catanionic Langmuir Monolayer. *J. Phys. Chem. Lett.* 1, 1936–1940.

Wilkinson, D.A., Tirrell, D.A., Turek, A.B., McIntosh, T.J., 1987. Tris buffer causes acyl chain interdigitation in phosphatidylglycerol. *Biochim. Biophys. Acta - Biomembr.* 905, 447–453.

Wu, F.G., Wu, R.G., Sun, H.Y., Zheng, Y.Z., Yu, Z.W., 2014. Demixing and crystallization of DODAB in DPPC-DODAB binary mixtures. *Phys. Chem. Chem. Phys.* 16, 15307–15318.